GLOBAL BIOGEOCHEMICAL CYCLES, VOL. 9, NO. 1, PAGES 121–137, MARCH 1995

Limiting future atmospheric carbon dioxide

Jorge L. Sarmiento and Corinne Le Quéré
Atmospheric and Oceanic Sciences Program, Princeton University, Princeton, New Jersey

Stephen W. Pacala
Department of Ecology and Evolutionary Biology, Princeton University, Princeton, New Jersey

Abstract. We estimate anthropogenic carbon emissions required to stabilize future atmospheric CO_2 at various levels ranging from 350 ppm to 750 ppm. Over the next three centuries, uptake by the ocean and terrestrial biosphere would permit emissions to be 3 to 6 times greater than the total atmospheric increase, with each of them contributing approximately equal amounts. Owing to the nonlinear dependence of oceanic and terrestrial biospheric uptake on CO_2 concentration, the uptake by these two sinks decreases substantially at higher atmospheric CO_2 levels. The uptake also decreases with increased atmospheric CO_2 growth rate. All the stabilization scenarios require a substantial future reduction in emissions.

Introduction

Estimates of future atmospheric CO_2 levels have generally been based on scenarios of fossil and land use emissions that are used to force a model of the atmosphere, ocean, and terrestrial biosphere [e.g., *Houghton et al.*, 1990]. Increased recognition of the importance of limiting future atmospheric CO_2 levels has led to a new strategy that begins with a given atmospheric CO_2 content as the goal, then uses models to deduce land and fossil use emission scenarios consistent with that goal. In preparation for new 1994 and 1995 reports the Intergovernmental Panel on Climate Change (IPCC) has organized a model comparison study using a wide range of ocean and terrestrial biosphere models to estimate allowable emissions for the prescribed set of future upper limit atmospheric CO_2 concentrations shown in Figure 1a [*Enting et al.*, 1994]. This paper describes our contribution to that study, with a major emphasis on explaining how the basic structure of the different CO_2 scenarios and our ocean and terrestrial models influences the oceanic and terrestrial uptake capacity.

The only interaction between the oceanic and terrestrial biospheric carbon cycles is indirectly through their respective impacts on the atmospheric CO_2 content. An attractive by-product of specifying atmospheric CO_2 content is that the ocean and terrestrial biosphere models can be run and analyzed completely independently of each other. We shall do that here, bringing the results together at the end in a discussion of deduced net sources. We begin with a section describing our oceanic and terrestrial models.

Paper number 94GB01779.
0886-6236/95/94GB-01779$10.00

Models

Ocean

Oceanic uptake of carbon is simulated with the world ocean general circulation model (OGCM) of *Toggweiler et al.* [1989], as modified by *Toggweiler and Samuels* [1993]. The model has a variable horizontal resolution averaging about 4°, and 12 vertical levels of variable thickness with maximum depth of 5000 m. It is forced with annual mean climatic winds from *Hellerman and Rosenstein* [1983]. Surface temperature and salinity are damped toward their observed annual mean climatic values obtained from *Levitus* [1982]. The model is run toward equilibrium for >15,000 years using a time step of 1/300 year.

Occanic uptake of CO_2 is predicted with the OGCM model using the perturbation approach of *Sarmiento et al.* [1992]. The equation for perturbation dissolved inorganic carbon (DIC) in the ocean is

$$\frac{\partial C}{\partial t} = -\vec{V}\cdot\vec{\nabla}C + \vec{\nabla}_h\cdot\left(D_h\vec{\nabla}_h C\right) + \frac{\partial}{\partial z}\left(\frac{D_v}{\vartheta}\frac{\partial C}{\partial z}\right) \qquad (1)$$

where $C = \delta\mathrm{DIC} = \mathrm{DIC} - \mathrm{DIC}_0$, and DIC_0 is the steady state DIC present in the ocean before anthropogenic additions began. V is velocity predicted by the GCM, and D is the subgrid scale diffusivity parameterization, with the subscripts h and v symbolizing horizontal and vertical, respectively. The vertical diffusivity varies smoothly from 0.3 $cm^2\ s^{-1}$ in the upper kilometer to 1.3 $cm^2\ s^{-1}$ in the deepest layer. Horizontal diffusivity decreases from 1.0×10^7 $cm^2\ s^{-1}$ at the surface to 0.5×10^7 $cm^2\ s^{-1}$ at the bottom. The parameter ϑ is 1 except when vertically adjacent layers are unstably stratified, in which case, ϑ=0 and the layers are convectively adjusted (i.e., homogenized with respect to each other).

No carbon fluxes are permitted across any of the boundaries except for the flux of CO_2 across the air-sea interface obtained from

$$f_{\delta CO_2} = k_g(1-\gamma_{ice})(\delta pCO_{2_{atm}} - \delta pCO_{2_{oc}}) \qquad (2)$$

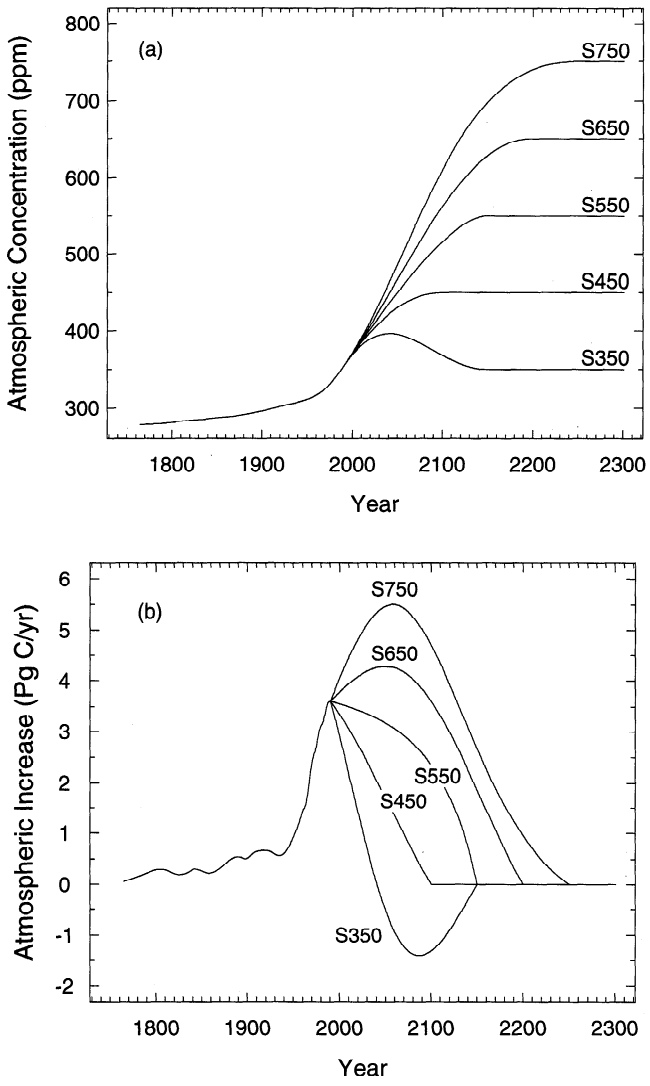

Figure 1. (a) Intergovernmental Panel on Climate Change (IPCC) scenarios for future atmospheric pCO_2 levels (see text for discussion of pCO_2). Prior to 1990 the curve shown is a smooth spline fit to observations [*Enting et al.*, 1994]. The labels on the curves give the final pCO_2 mixing ratio in parts per million. (b) The annual rate of increase of atmospheric pCO_2 calculated from the curves in Figure 1a.

where k_g is the gas exchange coefficient (we use the wind speed dependent formulation of *Wanninkhof* [1992], with wind speeds from *Esbensen and Kushnir* [1981]), γ_{ice} is the fraction of ice cover obtained from *Alexander and Mobley* [1976], and pCO_2 is the partial pressure of carbon dioxide corrected for the appropriate pressure in moist air at 100% water vapor saturation at the temperature of the surface water [cf. *Sarmiento et al.*, 1992]. The atmospheric perturbation $\delta pCO_{2_{atm}}$ is defined as $pCO_{2_{atm}}(t) - pCO_{2_{atm}}(0)$, with $pCO_{2_{atm}}(t)$ specified according to the IPCC scenarios of Figure 1 and $pCO_{2_{atm}}(0)$ set equal to 278 ppm, the approximate mean preindustrial mixing ratio.

The oceanic perturbation $\delta pCO_{2_{oc}}$ is calculated from oceanic δDIC using the same approximation as *Sarmiento et al.* [1992]

$$\frac{\delta pCO_{2_{oc}}}{\delta DIC} = z_0 + z_1 \delta pCO_{2_{oc}} \quad (3)$$

where

$$z_0 = 1.7561 - 0.031618 \times T + 0.0004444 \times T^2$$

and

$$z_1 = 0.004096 - 7.7086 \times 10^{-5} \times T + 6.10 \times 10^{-7} \times T^2$$

The equation for z_0 has a misprint in the original given by *Sarmiento et al.* [1992]; it was missing the 0 after the decimal in the second term on the right-hand side. T is temperature in degrees Celsius, DIC is in units of μmol kg^{-1}, and pCO_2 is in ppm. Note that if z_1 were 0, δpCO_2 and δDIC would be directly proportional to each other, i.e., their relationship would be linear. The nonlinearity in the relationship between these two properties is due to the fact that the uptake capacity of the ocean goes down as the amount of CO_2 increases. For every anthropogenic CO_2 molecule added to the ocean today that stays as CO_2 an additional ~20 anthropogenic CO_2 molecules react with carbonate ion to form bicarbonate ion via the reaction

$$CO_2 + CO_3^{2-} + H_2O \rightarrow 2HCO_3^-$$

The vast majority of the oceanic uptake capacity for anthropogenic CO_2 is thus due to this "bicarbonate buffer." However, as the amount of anthropogenic CO_2 in the ocean increases, the carbonate ion concentration is reduced and bicarbonate ion is increased. Thus a smaller portion of CO_2 molecules are able to follow this pathway.

The model used in this study differs in several respects from the original simulation described by *Sarmiento et al.* [1992]. Table 1 summarizes how these modifications affect the CO_2 uptake simulation. The combined changes to the circulation model include closing the Indonesian Straits, lengthening the salinity damping time constant to 120 days, and doing the CO_2 simulation "on-line." Sarmiento et al. took the physical model after it had been run out for 2009 years, then ran it an additional 55 years to produce time-averaged velocity fields and information on convection frequency which were used for an "off-line" simulation of the carbon uptake. The off-line simulation does not exactly reproduce the results of simulations that were done with the actual physical model on-line. Here we do the simulation on-line. The combined effect of these modifications to the circulation model is to reduce oceanic uptake by 0.5% (Table 1). We also used the gas exchange coefficient formulation of *Wanninkhof* [1992], rather than that of *Broecker et al.* [1985]. This reduces the 1980-1989 uptake a further 1.1%, for a total reduction of 1.6% below the *Sarmiento et al.* [1992] result (Table 1).

Terrestrial Biosphere

Future changes in the net flux of anthropogenic CO_2 between the terrestrial biosphere and the atmosphere will be caused by two separate processes. First, changes in land use will alter patterns of CO_2 release following anthropogenic disturbance (e.g., deforestation) and CO_2 uptake as disturbed lands recover.

Because future land use fluxes are specified in the IPCC scenarios, we do not require a dynamical model of land use here. Second, rates of CO_2 uptake and release by the terrestrial biosphere may respond to changes in atmospheric CO_2 levels (i.e., CO_2 fertilization), climate (i.e., temperature responses of photosynthesis, respiration, and decay), and nitrogen deposition (i.e., increased production or changes in litter chemistry in response to N fertilization).

Previous studies provide evidence that the terrestrial biosphere has already responded to one or more of these factors in the years since the industrial revolution [e.g., *Siegenthaler and Sarmiento*, 1993]. Uptake by the terrestrial biosphere has been identified as a probable cause of the so-called "missing sink" for anthropogenic carbon from 1850 to the present [*Siegenthaler and Sarmiento*, 1993]. Estimates of the missing sink have been produced by combining smoothed estimates of atmospheric CO_2 (Figure 2a), oceanic uptake (Figure 2c), fossil fuel production (Figure 2c), and land use (Figure 2c). The estimate by *Houghton* [1993] in Figure 2e shows a gradual increase in the missing carbon from near 0 before 1920 to a maximum in 1970, at which point the growth stalls and even reverses. The long period of growth followed by a stalling is intriguing, but we were concerned that it might contain artifacts of the smoothing of atmospheric CO_2 observations.

We therefore went back to the raw, deseasonalized atmospheric data shown in Figure 2b and used these to drive a new ocean uptake simulation. The results of this work, summarized in Figures 2d and 2f, give a different view of the terrestrial sink. Interannual variability is extremely large. A substantial cause of this prior to the initiation of the Mauna Loa time series in 1958 is inadequate sampling resolution and measurement error of ice core samples. By contrast, after 1958 the variability is real, as evidenced by corroborating measurements from other stations [*Boden et al.*, 1991], with a strong correlation to the El Niño-Southern Oscillation phenomenon [*Bacastow et al.*, 1980; *Keeling et al.*, 1989]. In addition, the period of near-zero terrestrial uptake now appears to extend well beyond 1920 to about 1940; followed by a brief period of growth between 1940 and 1950, after which the terrestrial uptake is roughly constant except for interannual variability.

In this paper we present a simple model of the response of the terrestrial biosphere to changes in temperature and atmospheric CO_2. We use published values for some of the model's parameters and estimate the remainder by fitting the model to the historical record of terrestrial uptake (missing carbon) in Figure 2f. During the fitting the model is forced by the atmospheric CO_2 record in Figure 2b and the global mean temperature record in Figure 3.

We then use the calibrated model to forecast the uptake of anthropogenic carbon under the IPCC scenarios for atmospheric CO_2 and three different kinds of temperature forcing caused by increased CO_2. First, global mean temperature is constant and set equal to ΔT at the beginning of the time series of Figure 3, -0.33°C relative to the 1951-1980 average. Second, we assume that temperature equilibrates instantaneously to atmospheric CO_2 using the 1990 IPCC relationships [*Houghton et al.*, 1990]. Specifically, radiative forcing (Q in W m^{-2}) due to CO_2 is $\Delta Q = 6.3 \ln(I_t^{atm} / I_0^{atm})$ where I_t^{atm} is the atmospheric inventory in year t and I_0^{atm} is the atmospheric inventory at the beginning of the scenario (1765). The equilibrium warming resulting from a change in radiative forcing is $\Delta T' = \Delta Q / L$, where L, the climate sensitivity parameter, is 1.8±0.7 W m^{-2} K^{-1}. This $\Delta T'$ is added to the initial -0.33°C value. Third, we assume that temperature equilibrates instantly to double the radiative forcing shown above, to account approximately for the contribution to radiative forcing from other anthropogenic greenhouse gases. The latter two cases are upper limits to the amount of warming that the radiative forcing would give, since the large oceanic heat capacity slows the rate at which the equilibrium is achieved.

The terrestrial biosphere model is illustrated in Figure 4. The boxes represent the state variables (carbon pools) of the model, and the annual change for each state variable is equal to the sum of the flux terms in and out of the appropriate box. For example, the equation for metabolic carbon B is:

$$dB/dt = (\mathrm{NPP})\ (0.65) - B/2\ \mathrm{yr} \qquad (4)$$

with net primary production NPP = 0.8 (GPP - $r_m e^{\nu \Delta T} B$), where r_m is rate of maintenance respiration and ν (deg^{-1}) is a temperature sensitivity coefficient. The model is linear with the exception of the term for gross primary production (GPP). This term is, perhaps, the most important in the model because it governs the flux into the biosphere and is thus responsible for terrestrial uptake of atmospheric carbon. GPP responds to the CO_2 concentration as well as temperature and includes the impact of increases in the size of the leaf canopy that occur as the terrestrial biosphere adjusts to increasing CO_2 and greenhouse warming. GPP is calculated as an integral through the canopy, as by *Raich et al.* [1991]

$$\mathrm{GPP} = \int_0^{B^*} P_{\max} e^{\lambda \Delta T} \left(\frac{\mathrm{CO_2}}{K_{\mathrm{CO_2}} + \mathrm{CO_2}} \right) \left(\frac{e^{-\alpha B}}{K_L + e^{-\alpha B}} \right) dB \qquad (5)$$

where B^* corresponds to the leaf layer obtained at the compensation point where photosynthesis equals respiration

Table 1. Sensitivity of Oceanic Uptake to Modifications in the Original Model of *Sarmiento et al.* [1992]

Model Version	Cumulative Carbon Uptake (1800-1990), Pg	Mean Uptake in 1980-1989, Pg yr^{-1}
Sarmiento et al. [1992]	109.8	1.86
Circulation model changes	109.2	1.85 (-0.5%)
This study	110.5	1.83 (-1.6%)

The percent deviations in the final column are relative to the *Sarmiento et al.* [1992] results of the top row. The present model takes up 1.6% less than the model of *Sarmiento et al.* [1992] during the 1980-89 decade. This is in contrast to the cumulative 1800-1990 carbon uptake, which is 0.6% higher owing to the fact that the initial pCO_2 for the Intergovernmental Panel on Climate Change study is 278 ppm, whereas *Sarmiento et al.* [1992] used 280 ppm.

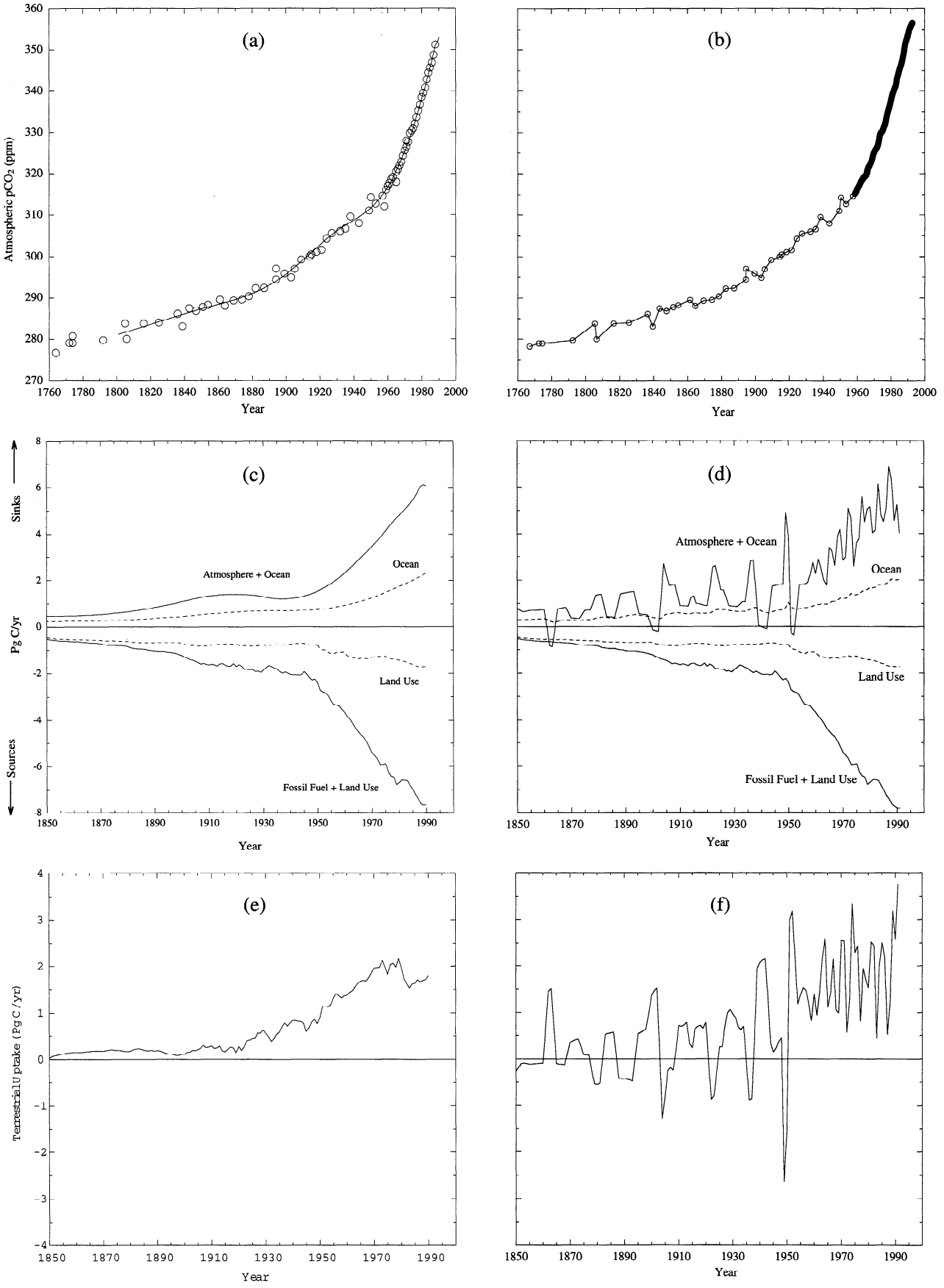
(a)
Atmospheric pCO2 (ppm)
Year
(b)
Year
(c)
Sinks
Sources
Pg C/yr
Atmosphere + Ocean
Ocean
Land Use
Fossil Fuel + Land Use
Year
(d)
Atmosphere + Ocean
Ocean
Land Use
Fossil Fuel + Land Use
Year
(e)
Terrestrial Uptake (Pg C/yr)
Year
(f)
Year

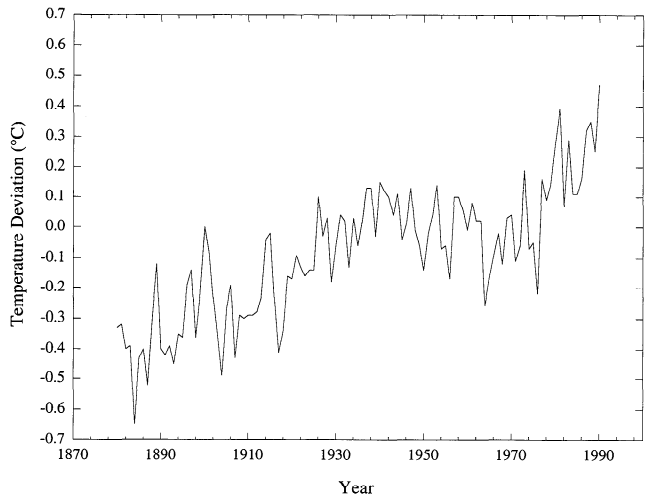

Figure 3. Annual mean temperature anomaly record used to force the terrestrial model. These data are an updated version of *Hansen and Lebedeff*'s [1987] record, provided to us by H. Wilson. The 1880 value of -0.33°C was used for the first 30 years of the model simulation beginning in 1850. The CO_2 used to force the terrestrial model is obtained from Figure 2b.

(plants are assumed to carry leaves only to the compensation point):

$$P_{\max} e^{\lambda \Delta T} \left(\frac{CO_2}{K_{CO_2} + CO_2} \right) \left(\frac{e^{-\alpha B^*}}{K_L + e^{-\alpha B^*}} \right) = r_m e^{\nu \Delta T}$$

Note that the expression for GPP in (5) contains a double Michaelis-Menten relationship. The first such term $[CO_2 / (K_{CO_2} + CO_2)]$ governs CO_2 dependence (with half-saturation constant K_{CO_2}), and the second governs shading (with half-saturation constant K_L = 0.25) [see *Raich et al.*, 1991; *Larcher*, 1980]. In the second Michaelis-Menten relationship, α should be viewed as the product of the light extinction coefficient and a constant giving the ratio of leaf metabolic carbon to total carbon contained in and supporting leaves. $P_{\max}$ governs the maximum rate of photosynthesis, r_m governs the rate of maintenance respiration, and $e^{\lambda \Delta T}$ and $e^{\nu \Delta T}$ describe, respectively, the dependence of photosynthesis and maintenance respiration on temperature change ΔT, defined with respect to the 1951-1980 mean (Figure 3). Finally, the constant 0.8 that multiplies the expression for NPP represents the fraction of NPP remaining after construction costs (growth respiration [*Raich et al.*, 1991]).

The $e^{\nu \Delta T}$ term also governs the temperature sensitivity of decomposition rates of litter (D_B and D_W) as well as soil S (see Figure 4), because these are controlled by heterotrophic respiration [*Raich et al.*, 1991]. Although we assume that the temperature sensitivity of photosynthesis is concave up ($e^{\lambda \Delta T}$), empirical studies typically report more complex functions that are concave down over at least part of the temperature range [*Larcher*, 1980]. However, the range of temperatures in this study is sufficiently small to ensure approximate linearity of both the function used here and relationships reported elsewhere. We employ the simple function $e^{\lambda \Delta T}$, rather than a more complex relationship, to facilitate comparison with the temperature dependence of respiration and decay. Also note that total plant maintenance respiration is proportional to metabolic carbon B but not structural carbon W because respiration rates associated with maintaining structural tissue are low, in particular because of dead heartwood in living forest trees [*Ryan*, 1991]. We investigated a version of the model in which maintenance respiration was equal to $r_m(B + \gamma W)e^{\nu \Delta T}$, but this addition did not result in significantly better fits, and goodness of fits was insensitive to the value of the constant γ. This is because the ratio B/W undergoes only small fluctuations over the time series.

Although the nonlinear dependence of GPP on B is appropriate for light limitation, it might be inappropriate for limitation by nutrients or water. For this reason, we also investigated a version of the model in which the above expression for GPP was multiplied by $1/(1+\phi B^{\theta})$ where ϕ and θ are fitted constants. However, the additional density dependence did not substantially improve the fits obtained (the coefficient of determination R^2 never increased by more than 1 percentage point), and estimates of ϕ and θ were such that the additional term was approximately constant over the full time series.

Figure 2. (a) and (b) Observations of atmospheric CO_2 increase. Data prior to 1958 are from trapped air bubbles in the South Pole [*Siegenthaler et al.*, 1988] and Siple ice cores [*Neftel et al.*, 1982; *Friedli et al.*, 1986]. After 1958 we show in Figure 2a, the annual mean of monthly measurements made at Mauna Loa [*Keeling and Whorf*, 1991], and in Figure 2b, monthly values obtained after deseasonalizing the data with a 12-month smoothing. (c) and (d), Anthropogenic carbon sources and sinks. The ocean uptake in Figure 2c is obtained from an ocean GCM model forced with the spline fit to the data in Figure 2a *Sarmiento et al.* [1992]. The ocean uptake in Figure 2d is obtained by a new simulation with the same model but forced with the raw data in Figure 2b linearly interpolated between measurements. The atmospheric increase in Figure 2c is calculated from the spline fit in Figure 2a, and the annual mean atmospheric increase in Figure 2d is calculated from the linearly interpolated data in Figure 2b. Fossil fuel production [*Marland et al.*, 1989] and land use [*Houghton*, 1993] are the same in Figures 2c and 2d. These data are available in annual increments only. (e) and (f), The annual terrestrial uptake estimated from the residual of the curves in Figures 2c and 2d, respectively. The integrated sources from 1850 to 1990 are 219 Pg of carbon for fossil fuel and 122 Pg for land use. The atmospheric increase is 143 Pg in both Figures 2c and 2d, and the oceanic increase is 101 Pg in Figure 2c, and 100 Pg in Figure 2d. The cumulative terrestrial uptake from 1850 to 1990 is thus estimated to be 97 Pg in Figure 2e and 98 Pg in Figure 2f.

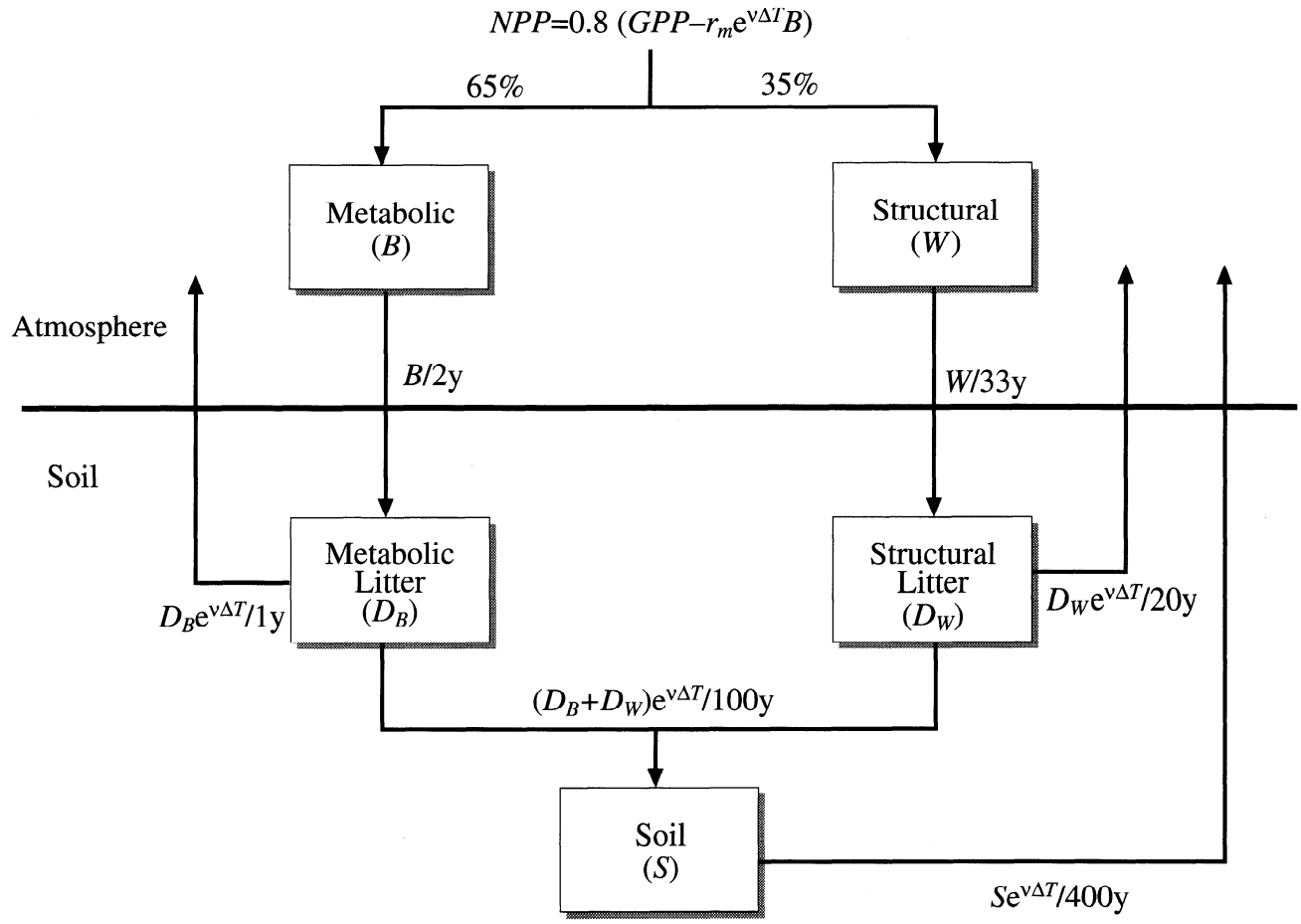

Figure 4. Terrestrial biosphere model. See text for explanation.

The values of P_{max}, K_{CO_2}, α, r_m, λ, and ν shown in Table 2 were estimated by minimizing least squares deviations from the terrestrial uptake time series (Figure 2f). We performed two separate fits, one for all years corresponding to actual measurements of atmospheric CO_2 (either directly or from glacial ice, Figure 5a) and one for 1958-present (the years with more reliable direct measurements of atmospheric CO_2, Figure 5b). We used the Metropolis algorithm to find the minimum [*Metropolis et al.*, 1953; *Szymura and Barton*, 1986]. To prevent the estimator from searching unrealistic parameter space, the search was confined to values yielding a terrestrial net primary productivity (*NPP*) of 60 Pg of carbon in the final year of the time series (1991). All remaining parameters in Figure 4 were specified a priori using published estimates [*Amthor*, 1984; *Bolin*, 1986; *Cannell*, 1982; *Emmanuel et al.*, 1981; *Emmanuel et al.*, 1984; *Larcher*, 1980; *Olson et al.*, 1983; *Parton et al.*, 1987; *Parton et al.*, 1988; *Post et al.*, 1990; *Raich et al.*, 1991; *Rastetter et al.*, 1991; *Schimel et al.*, 1991; *Taylor and Lloyd*, 1992; *Zinke et al.*, 1986].

Parameter estimates obtained through the fitting procedure were virtually identical to independent measurements reported in small-scale field and laboratory studies (Table 2). For example, our estimate of β (the fractional increase of productivity resulting from a doubling of atmospheric CO_2) was 0.36 for the fits from 1958 to the present, compared with a mean of ~0.35 in field and laboratory studies [*Bazzaz*, 1990; *McGuire et al.*, 1992; *Taylor and Lloyd*, 1992]. The corresponding estimate of the Q_{10} of respiration (the fractional increase of respiration in response to a 10°C warming) was 2.36, compared with a mean of 2.4 in published empirical studies [*Raich and Schlesinger*, 1992]. The inventories and fluxes predicted by the model (Table 2) are all within the range of published estimates [*Bolin*, 1986; *Emmanuel et al.*, 1984; *Larcher*, 1980; *McGuire et al.*, 1992.; *Olson et al.*, 1983; *Post et al.*, 1990; *Raich et al.*, 1991; *Taylor and Lloyd*, 1992; *Zinke et al.*, 1986]. Finally the fitted model accounted well for both the long-term trend and interannual variability of the missing sink (Figure 5). In what follows we use parameter estimates obtained from the fit using years 1958 to the present. Similar results are obtained using the fit for the entire industrial period.

Results

Oceanic Uptake

Figure 6 shows oceanic uptake for the IPCC scenarios. We will discuss in detail the processes that determine the uptake

Table 2. Results of the Model Fit to the Terrestrial Uptake Estimate

	Fit to Data From 1850 to 1991	Fit to Post-1958 Data
NPP parameters obtained from fit		
P_{max}, Pg yr^{-1}	5.3	5.9
K_{CO_2}, ppm	324 (equivalent to β=0.32)	383 (equivalent to β=0.36)
α, Pg^{-1}	0.042	0.039
r_m, yr^{-1}	0.31	0.39
Temperature sensitivity parameters obtained from fit		
ν, deg^{-1}	0.071 (equivalent to Q_{10}=2.03)	0.086 (equivalent to Q_{10}=2.36)
λ, deg^{-1}	0.046 (equivalent to Q_{10}=1.59)	0.043 (equivalent to Q_{10}=1.54)
Coefficient of determination		
R^2	0.44	0.43
Inventories in 1991 predicted by model*, Pg		
B	77 (13)	77 (15)
W	643 (78)	639 (85)
D_B+D_W	346 (27)	343 (28)
S	1297 (16)	1217 (18)
Fluxes in 1991 predicted by model, Pg C yr^{-1}		
GPP	99	105
NPP	60	60
GPP-NPP	39	46

See Figure 4 and the text for a definition of symbols. The first 6 parameters are obtained by fitting the estimated missing sink prior to 1991 subject to the constraint that net primary production (NPP)= 60 Pg yr^{-1} in 1991. The remaining numbers given in the table are model predictions.

*Numbers in parentheses are the increase from 1850 to 1991.

for the S450 and S750 scenarios, as these represent reasonable lower and upper limits. S350 is lower than S450, but it requires a reduction of atmospheric CO_2 (Figure 1b), which we do not believe is realistic.

A useful diagnostic of how much the oceanic uptake contributes to the total carbon budget is the airborne fraction for the combined atmosphere and ocean:

$$AF_{ao}(t) = \frac{(I_t^{atm} - I_0^{atm})}{(I_t^{atm} - I_0^{atm}) + (I_t^{oc} - I_0^{oc})} \quad (6)$$

where I^{atm} is the atmospheric CO_2 inventory, and I^{oc} is the oceanic inventory in Pg of carbon, and t=0 is the beginning of the simulation in 1765. The airborne fraction for S450 is lower than that for S750 throughout the entire time span after 1990 (Figure 7). By the year 2300, S750 has an airborne fraction more than 0.11 greater than S450. This difference is almost a third of the S450 airborne fraction.

There are two reasons that the S750 airborne fraction is so much higher than in S450. The most important is that the proportion of CO_2 molecules able to react with carbonate ions and water to form bicarbonate ions is reduced by a larger amount in S750. With the higher oceanic uptake of the S750 scenario (Figure 6) the concentration of CO_3^{2-} is reduced and HCO_3^- increased by a greater amount than in S450, thus a smaller fraction of the CO_2 molecules can follow this pathway. Figure 8a shows how the instantaneous gradient, $\partial DIC / \partial CO_{2_{oc}}$, calculated from (3) varies in time for the two models (the instantaneous gradient is different from the cumulative gradient $\delta DIC/\delta pCO_2$). The instantaneous gradient decreases from its preindustrial value of greater than 20 to just over 17 in 1990 and 11 by the end of the S450 simulation and just over 5 by the end of the S750 simulation. By the year 2300 the oceanic uptake capacity associated with seawater chemistry in the S750 simulation is less than half that of the S450 simulation for a given CO_2 increment. Figure 7 and 8b show what happens when the chemistry equation is linearized (z_1=0 in (3)) so as to remove the effect of CO_3^{2-} ion reduction. The scenarios with linearized chemistry have a higher oceanic uptake than the simulations with nonlinear chemistry (Figure 8b). The effect is particularly large in the S750 scenario. As a consequence, the airborne fraction is much lower with linearized chemistry, and the difference in airborne fraction between the S450 and S750 scenarios is greatly reduced (Figure 7).

The remainder of the difference between the airborne fraction of S750 and S450 is a consequence of the time history of atmospheric CO_2. The slower rate of increase in S450 means

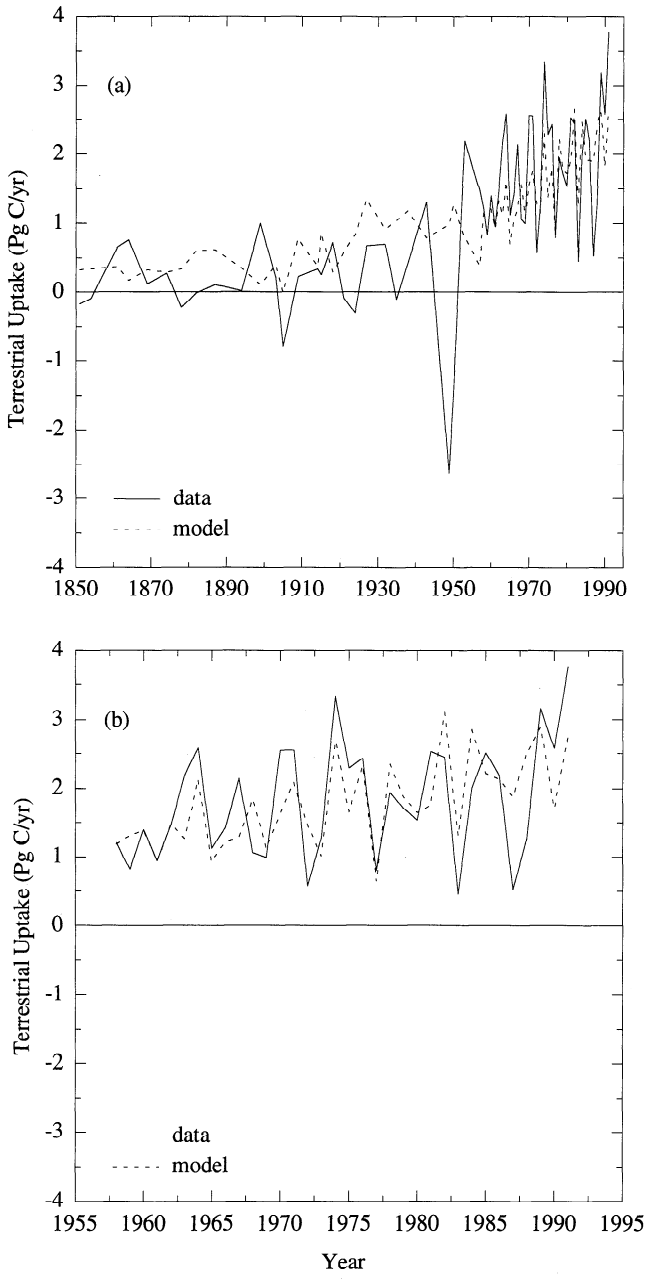

Figure 5. Results of model fits to the terrestrial sink. (a) Model forced to fit the entire data set from 1850 onward. (b) Model fitted to only the data after 1958, when the Mauna Loa observations were initiated. The cumulative terrestrial uptake from 1850 to 1990 calculated with the model is 132 Pg in Figure 5a and 146 Pg in Figure 5b, as compared with the data estimate of 98 Pg. The difference between the model and data is due mainly to the period prior to 1958, where our estimate of terrestrial uptake is most uncertain.

that a larger volume of the ocean interior will have time to exchange with the mixed layer for a given fractional increase in atmospheric CO_2. We can quantify the importance of the rate of atmospheric growth in controlling the airborne fraction by defining a mean CO_2 age for the atmospheric component as:

$$\text{Age}(\tau) = \frac{\int_0^\tau \left(I_t^{\text{atm}} - I_0^{\text{atm}}\right) dt}{\left(I_\tau^{\text{atm}} - I_0^{\text{atm}}\right)} \tag{7}$$

where I^{atm} stands for the atmosphere inventory. Figure 9a shows this mean age plotted versus time. Note that whether the ocean chemistry is linearized or not makes no difference to the age. As expected, S450 has an older mean age at all times than does S750. Plotting the airborne fraction versus mean age as in Figure 9b shows that the simulations with linearized chemistry fall almost directly on top of each other. Thus mean age serves as an excellent proxy for the processes other than chemistry, such as mixing and circulation, that account for the remaining difference between S450 and S750.

A final point concerns the timing of the peak in oceanic uptake (Figure 10). The S450 peak, which is only about 0.5 Pg yr^{-1}, above the 1990 uptake of 2.0 Pg yr^{-1}, occurs in 2026, delayed from the peak in the atmospheric increase rate by 36 years (Figure 10a). The S750 peak of about 4.0 Pg yr^{-1} occurs in 2085, 27 years after the peak in atmospheric increase rate (Figure 10b). In all the scenarios, oceanic uptake continues to grow even after the increase rate of atmospheric CO_2 has begun to drop.

The reason for the continuation of the positive trend in oceanic uptake beyond that in the growth rate of atmospheric CO_2 is that the trend in oceanic uptake is dependent on the trend in atmospheric CO_2 content, not the rate of growth of this trend. The following analytical approximation provides useful insight. We have firstly a carbon balance for the atmosphere

$$\frac{\partial C(t)}{\partial t} = S(t) - U(t) \tag{8}$$

where S is the source per unit time of carbon to the atmosphere and U is the oceanic uptake. We represent the atmospheric concentration as the integral of a series of infinitesimal pulse inputs to the atmosphere, multiplied by a Green's function

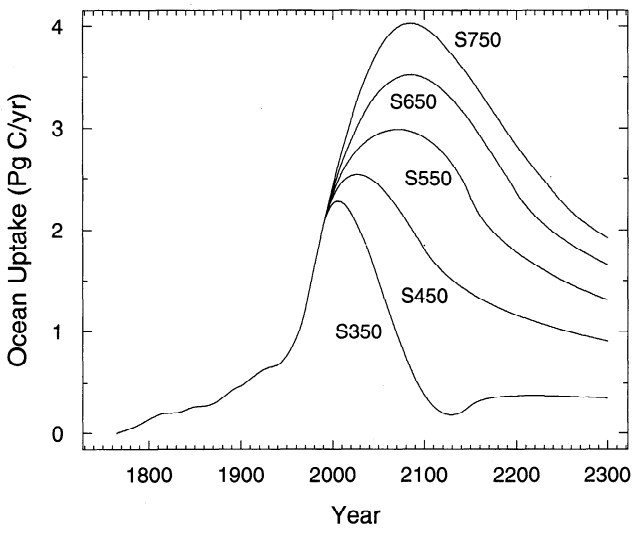

Figure 6. Annual oceanic uptake estimates for the IPCC scenarios of Figure 1a.

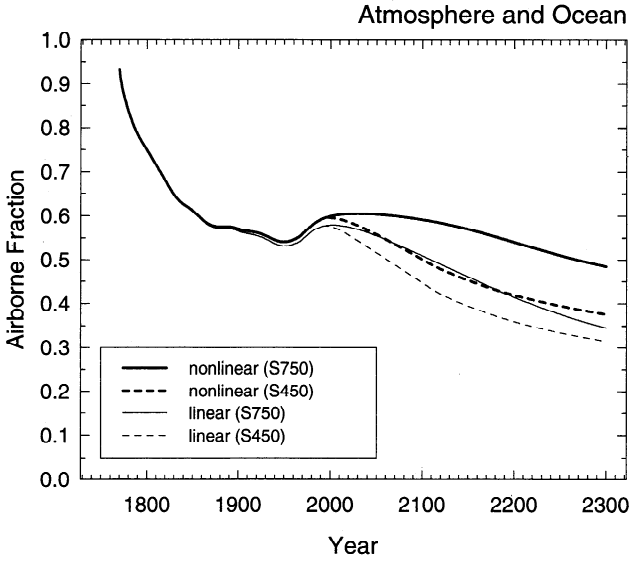

Figure 7. The airborne fraction for the combined atmosphere and ocean carbon content as a function of time. The nonlinear curves have the full oceanic chemistry effect given by equation (3). The linear curves have z_1=0.

which gives the fraction of that pulse that remains in the atmosphere after a given time has elapsed.

$$C(t) = \int_0^t S(\tau)G(t-\tau)d\tau + C_0$$

$$G(t) = a_0 + a_1 e^{-t/T_1} \tag{9}$$

C_0 is the initial atmospheric concentration. $S(\tau)$ is the pulse of carbon input to the atmosphere that occurs at time τ. The Green's function $G(t-\tau)$ is the fractional amount of $S(\tau)$ that remains in the atmosphere at time t; the remainder goes into the ocean. $G(t-\tau)$=1 at $t-\tau$=0. A sum of about 5 terms approximates the Green's function of ocean GCM models more closely [cf. *Maier-Reimer and Hasselmann*, 1987], but complicates the analytical solution. Note also that it is difficult to account for the nonlinearity of carbon system chemistry with the Green's function approach. When nonlinear carbon chemistry is included, the magnitude of the coefficients depends on the size of the pulse as well as the initial atmospheric CO_2 concentration and the time history of the background atmospheric CO_2 concentration onto which the pulse is imposed. Both *Maier-Reimer and Hasselmann* [1987] and *Sarmiento et al.* [1992] show results which illustrate the sensitivity of the Green's functions to the magnitude of the pulse.

What we wish to do is obtain an expression for $\partial U(t)/\partial t$. Differentiating (9) with respect to time gives

$$\frac{\partial C(t)}{\partial t} = S(t) + \int_0^t S(\tau)G'(t-\tau)d\tau \tag{10}$$

$$\frac{\partial C(t)}{\partial t} = S(t) - \frac{1}{T_1}\int_0^t S(\tau)G(t-\tau)d\tau + \frac{a_0}{T_1}\int_0^t S(\tau)d\tau \tag{11}$$

$$\frac{\partial C(t)}{\partial t} = S(t) - \frac{C(t)-C_0}{T_1} + \frac{a_0}{T_1}\int_0^t S(\tau)d\tau \tag{12}$$

where we have made use of the relationship $G'(t-\tau) \equiv \partial G(t)/\partial t = -(G(t)-a_0)/T_1$ in going from (10) to (11), and the definition of $C(t)$ given by (9) in going from (11) to (12). Substitution of (8) into (12) gives

$$U(t) = \frac{C(t)-C_0}{T_1} - \frac{a_0}{T_1}\int_0^t S(\tau)d\tau$$

$$\text{i.e., } \frac{\partial U(t)}{\partial t} = \frac{1}{T_1}\left(\frac{\partial C(t)}{\partial t} - a_0 S(t)\right) \tag{13}$$

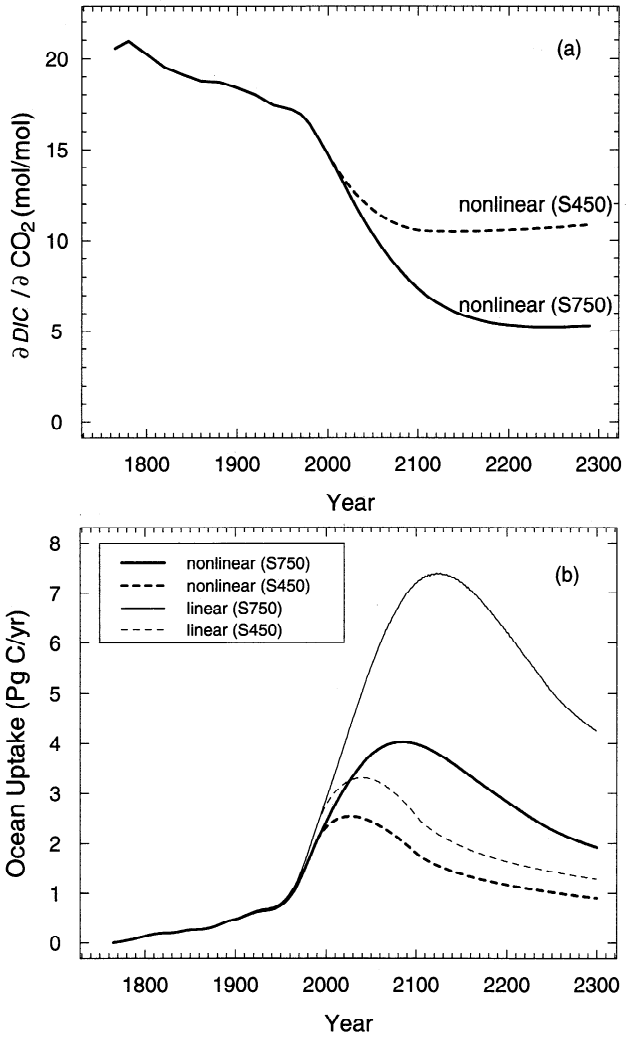

Figure 8. (a) The global mean instantaneous change in oceanic dissolved inorganic carbon (DIC) resulting from a given change in CO_2 concentration for the S450 and S750 scenarios. The mean is obtained by weighting the ratio at each model grid point by the air-sea flux of anthropogenic carbon. The sawtooth pattern before 2000, and rise in the ratio towards the end of the simulation result from the shifting pattern of the flux of CO_2 into the ocean and the fact that warm waters have a lower ratio than cold waters. The large reduction in this ratio through time is a measure of the reduction in the oceanic bicarbonate buffer of surface waters. (b) The annual ocean uptake for the S450 and S740 scenarios. The nonlinear curves have the full oceanic chemistry effect given by equation (3). The linear curves have z_1=0.

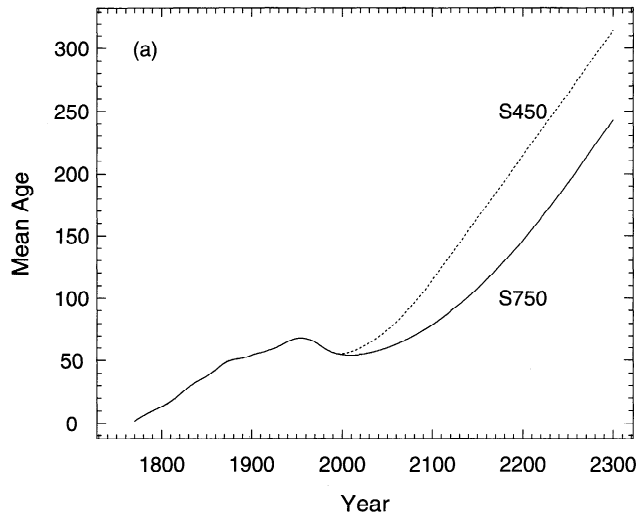

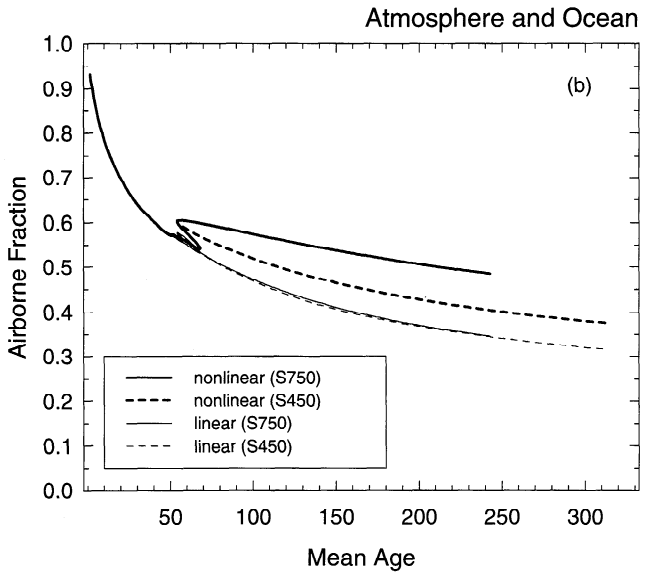

Figure 9. (a) Mean age of the atmospheric CO_2 perturbation as calculated by equation (7). (b) The airborne fractions of Figure 7 plotted versus mean age.

from which we see, as stated above, that the time dependence of U has the same sign as the time dependence of C. This continues to be the case until the increase rate goes below the fraction of the source function that remains permanently in the atmosphere, $a_0 S(t)$.

Terrestrial Uptake

Figures 11a and 11b show the terrestrial uptake predicted for the S450 and S750 scenarios, respectively, with the three different kinds of temperature forcing. The small "sawtooth" feature around year 2000 is caused by B becoming larger than B^* in (5). Equilibrium temperature estimates are shown in Figure 12. Note that terrestrial uptake decreases as temperature increases from a peak uptake of 4.7 Pg yr^{-1} with no temperature forcing in S750 to 2.9 Pg yr^{-1} with doubled temperature forcing and from a peak of 3.7 Pg yr^{-1} with no forcing in S450 to 2.7 Pg yr^{-1} with doubled forcing. Similarly, terrestrial uptake in the year 2300 decreases from 1.53 to 0.23 in S750 and from 0.73 to 0.26 in S450.

The effect of warming on terrestrial uptake is caused in large part by increased decomposition in the slowly decomposing soil compartment S. For example, Figure 13 shows uptake by the soil compartment in S750. Note that the differences between the curves in Figure 13 account for nearly all the differences between the curves in Figure 11b. Temperature effects are dominated by the soil compartment for three reasons. First, the soil compartment represents the single largest reservoir of terrestrial carbon (e.g., Figure 14). Second, living structural carbon W is the second largest pool in the model. Because the death rate of W is independent of temperature (unlike the mineralization rate of S), changes in temperature have a greater effect on S than on W. Third, the slow dynamics of the soil compartment ensure that it dominates terrestrial uptake in the latter part of each scenario.

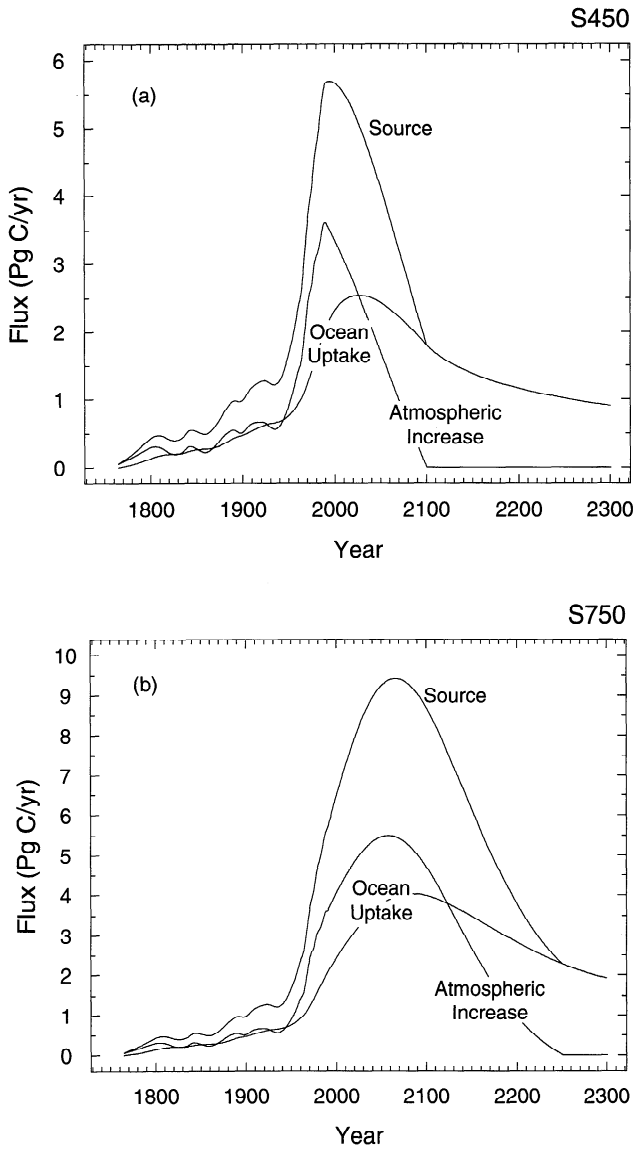

Figure 10. Annual fluxes of anthropogenic CO_2 in (a) the S450 scenario and (b) the S750 scenario.

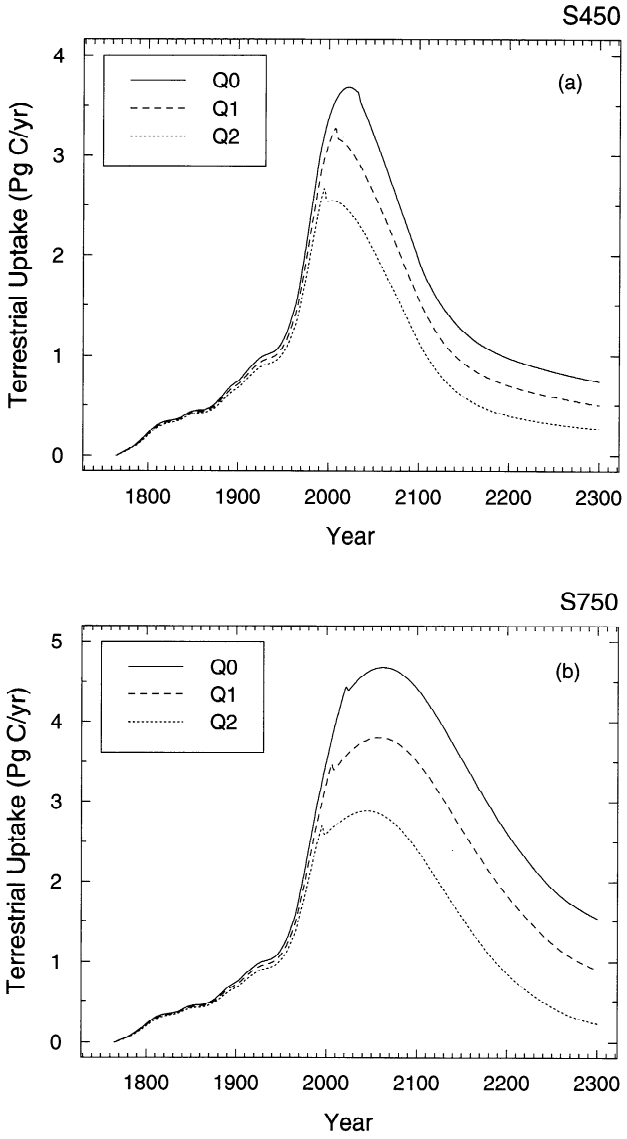

Figure 11. Terrestrial uptake in the (a) S450 and (b) S750 scenarios. Three uptake estimates are shown, one with no change in temperature (Q0), a second with the equilibrium warming that would result from the increase in CO_2 (Q1), and a third with the equilibrium warming that would result from twice the CO_2 radiative forcing (Q2).

For example, with no temperature forcing, virtually all terrestrial uptake is caused by increases in S after year 2100 in the S450 scenario and after year 2150 in the S750 scenario (Figures 14a and 14b).

The remainder of this section parallels the analysis of oceanic uptake in the preceding section. The airborne fraction for the combined atmosphere and terrestrial biosphere analogous to (6) is

$$AF_{ab}(t) = \frac{(I_t^{atm} - I_0^{atm})}{(I_t^{atm} - I_0^{atm}) + (I_t^b - I_0^b)} \qquad (14)$$

where I_t^b is the inventory of carbon (in petagrams) in the terrestrial biosphere in year t. Like (6), the airborne fraction (14) is lower in the S450 scenario than in the S750 scenario for years after 1990. This effect is largest in cases with no temperature forcing (Figure 15) but is present in all cases. There are two reasons that the S750 airborne fraction is considerably higher than the S450 fraction. First, the Michaelis-Menten dependence of terrestrial GPP on atmospheric CO_2 represents a nonlinearity directly analogous to the nonlinear chemistry of the bicarbonate buffer in the oceans. When the linear dependence of GPP on atmospheric CO_2 shown in Figure 16 is substituted for (5), the differences between the S450 and S750 airborne fractions decrease substantially (see Figure 15).

Second, as with the oceans, the time course of atmospheric CO_2 increase provides more time for the terrestrial biosphere to proceed toward its new steady state in the S450 scenario than in the S750 scenario. Figure 17 plots the airborne fractions against the mean age of atmospheric CO_2 defined by (7). Note that S450 has an older mean age than S750 and that the curves for linearized GPP fall almost on top of one another, exactly as in the corresponding plot for the ocean-atmosphere (Figure 9b). Thus mean age accounts for differences between the S450 and S750 scenarios not accounted for by nonlinear GPP.

Note in Figure 11 that the time of peak uptake by the terrestrial biosphere decreases as temperature forcing increases. In the S450 scenario the decrease is from year 2022, with no temperature forcing to 1995 with doubled forcing. In the S750 scenario the decrease is from 2062 with no forcing to 2045 with doubled forcing. Peak uptake occurs earlier in runs with increased temperatures simply because warming increases rates of carbon loss (respiration and decomposition) more than it increases rates of carbon gain (photosynthesis) (see the Q_{10} values in Table 2).

Recall that the atmospheric increase peaks in year 1990 in the S450 and year 2059 in S750. Why is it that without any temperature forcing the peak uptake by the terrestrial

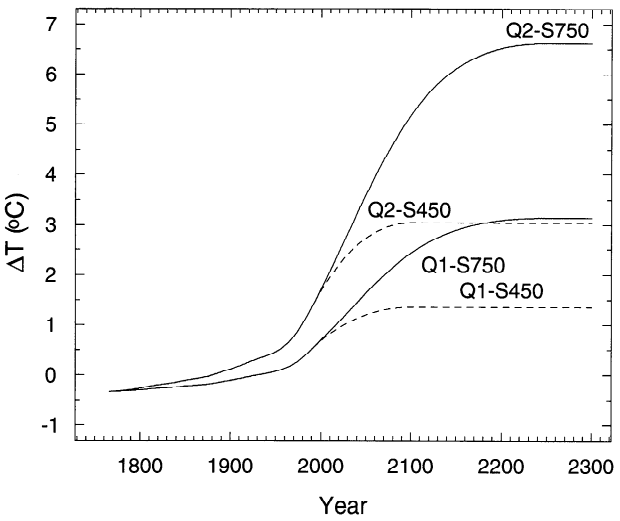

Figure 12. Equilibrium temperatures corresponding to the warming scenarios of Figure 11. These are given as temperature ΔT changes with respect to the 1951-1980 average. The initial ΔT is -0.33°C.

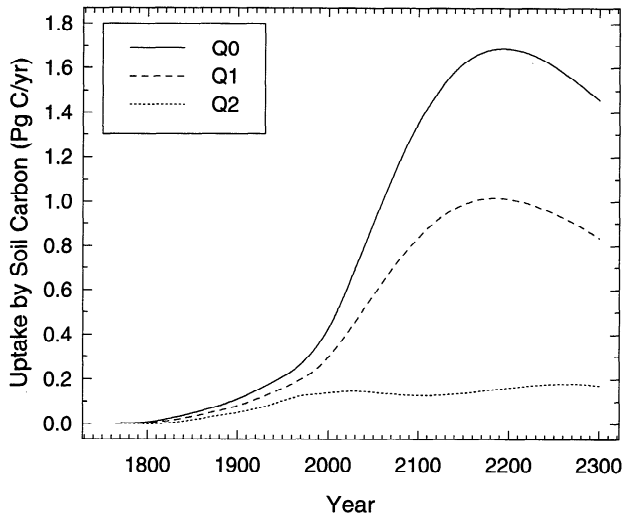

Figure 13. Soil carbon uptake in the S750 scenario. The warming scenarios are as in Figure 11. Soil uptake is very sensitive to the amount of warming permitted because of the impact of this on the rate of decomposition.

biosphere occurs 32 years later than the peak of the atmospheric increase in S450 and 3 years later in S750? Each equation of the biospheric model has the following form (see Figure 4):

$$\frac{dY(t)}{dt} = X(t) - aY(t) \tag{15}$$

where $Y(t)$ is a carbon pool, $X(t)$ is the input to the pool, and $-aY(t)$ is the loss from the pool.

After differentiating both sides of (15) with respect to time and rearranging, we have:

$$Y(t)'' + aY(t)' = X(t)' \tag{16}$$

where a single prime indicates a first time derivative and a double prime indicates a second time derivative. Now suppose that both $Y(t)$ and $X(t)$ are sigmoidal functions (see Figure 14), each with a single inflection point (i.e., $Y(t)''$ and $X(t)''$ are monotonically decreasing). Because $aY(t)' = X(t)'$ at the inflection point of $Y(t)$, $aY(t)' > X(t)'$ after the inflection point, and $aY(t)' < X(t)'$ before the inflection point, the maximum uptake by the carbon pool $Y(t)$ occurs after the maximum of $X(t)'$. Moreover, the magnitude of this time lag depends on the size of the constant a, which, in turn, governs the time scale of the dynamics of $Y(t)'$. In the limit of fast dynamics (as a approaches infinity), $aY(t)'$ equals $X(t)'$, and so the time lag between peak uptake and the maximum of $X(t)'$ approaches zero. In the limit of slow dynamics (as a approaches zero), $Y(t)''$ equals $X(t)'$, and so the time lag becomes infinitely long ($Y(t)'$ reaches its maximum only when $X(t)$ reaches its asymptote).

Considering first the equation for living metabolic carbon, (4), we have $Y(t) = B$, $X(t) = 0.65 \times 0.8 \times \mathrm{GPP}$, and $a = (0.65 \times 0.8 \times 0.39 \times e^{\nu \Delta T} - 0.5)\ \mathrm{yr}^{-1}$. Because a is relatively large, we expect that the peak of uptake by B will lag only slightly behind the inflection point of GPP. Moreover, because GPP is a concave down function of atmospheric carbon (see Figure 16), the inflection point of GPP occurs before the maximum rate of atmospheric increase; GPP′ is largest in 1988 in S450 and in 2015 in S750. Thus the maximum uptake by B should occur substantially before the maximum atmospheric increase, at least in the S750 scenario. This expectation is in fact true; B' is greatest in year 1989 of S450 and in year 2015 of S750.

Turning now to living structural carbon, we have $Y(t) = W$, $a = 0.03$, and, using the approximation that $B(t) = 0.52$ GPP/0.70 (see Figure 18), $X(t) = 0.20 \times$ GPP. Because a is relatively small, we expect the peak of uptake by W to lag behind the inflection point of GPP; but again, the lag is keyed to the inflection point of GPP, not the inflection point of atmospheric carbon. Uptake by W reaches its maximum 23 years after the maximum of GPP′ in S450 and 7 years after the maximum of GPP′ in S750.

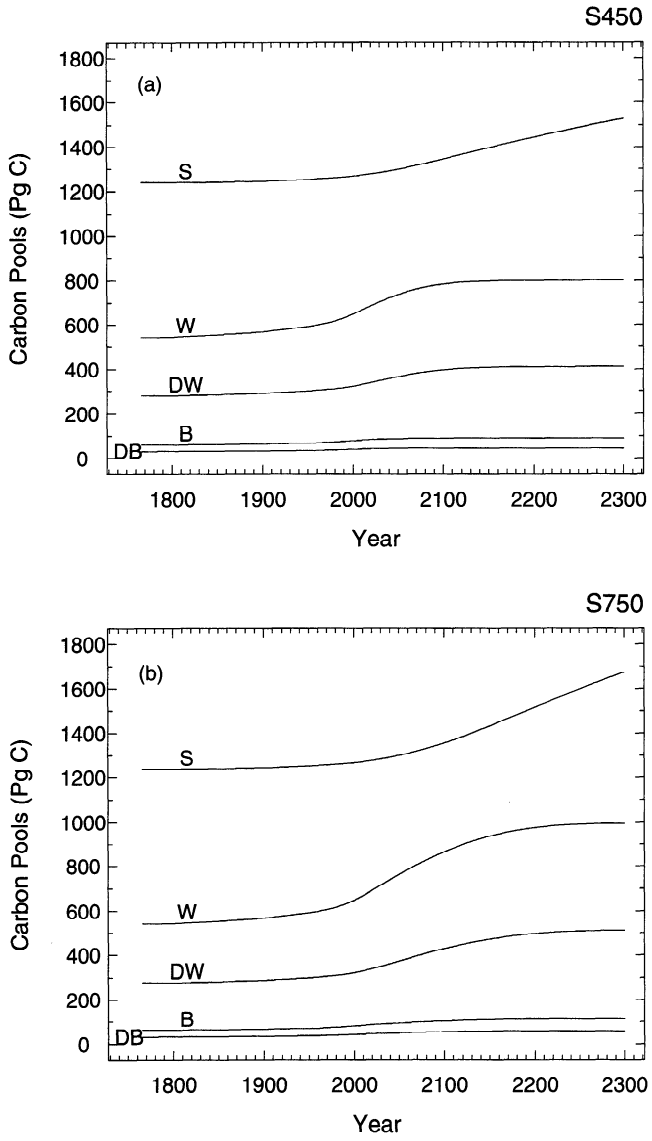

Figure 14. Time history of the terrestrial carbon pools in the (a) S450 and (b) S750 scenarios.

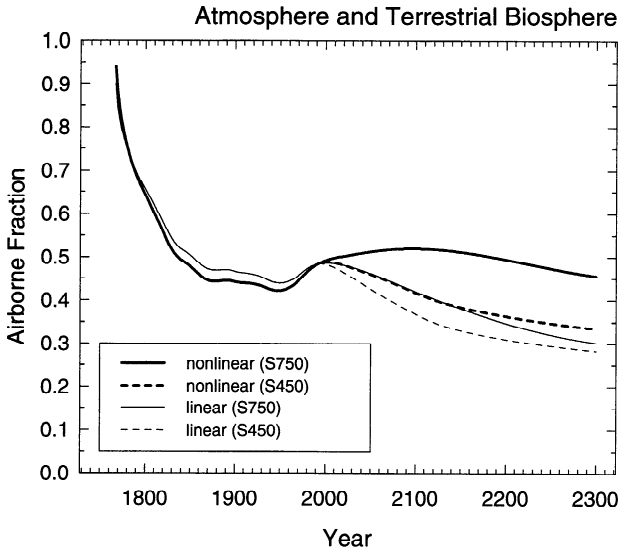

Figure 15. The airborne fraction for the combined atmosphere and terrestrial carbon content as a function of time. The nonlinear curves have the Michaelis-Menten CO_2 sensitivity given by equation (5). The linear curves replace the Michaelis-Menten dependency with a linear dependency (see Figure 16).

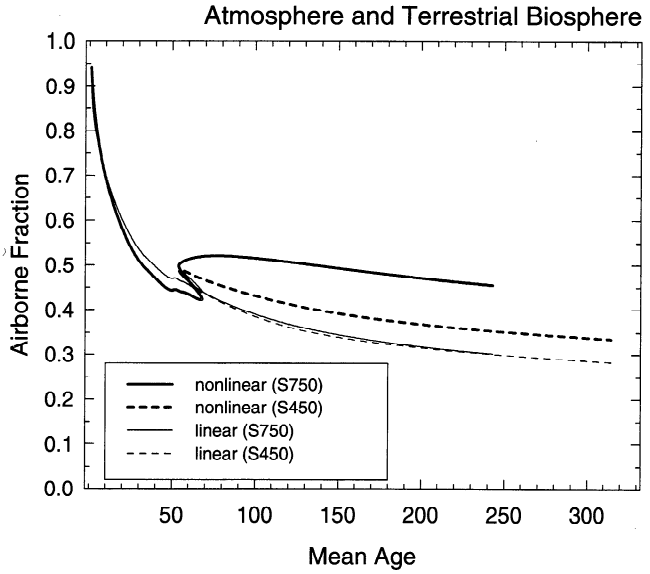

Figure 17. Airborne fraction for the terrestrial uptake simulations of Figure 15 plotted versus mean age.

After applying this method to the remaining compartments of the terrestrial biosphere, we find that uptake by D_B should peak close to the maximum of GPP′ because of the rapid turnover of D_B (actual = 1990 in S450 and 2016 in S750). Uptake by D_W should peak after the maximum uptake by W (actual = 2030 in S450 and 2054 in S750), and uptake by S should peak substantially after the maximum uptake by D_W (actual = 2119 in S450 and 2192 in S750).

In general, uptake by the biosphere tracks GPP′ with a series of time lags, each set by the time scale of death or decomposition. Although GPP′ peaks before the maximum of atmospheric increase, the time lags associated with the largest compartments of the terrestrial biosphere (W, D_W, and S) cause terrestrial uptake to peak after the maximum of the atmospheric increase. Finally, note that a simple extension of this method may be applied to cases with temperature forcing. The principle difference is that $Y(t)'$ in (15) must be replaced by $[a(t)Y(t)]'$ because the loss rate a changes over time owing to changes in temperature.

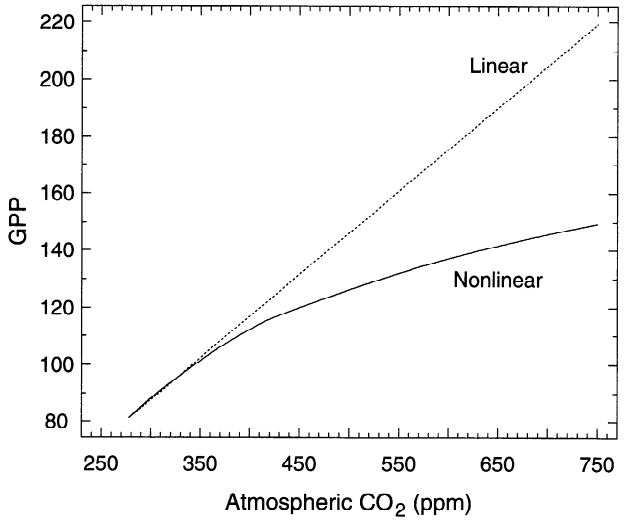

Figure 16. The solid line shows the dependence of gross primary production (GPP) on the CO_2 concentration given by equation (5). Also shown in the dashed line is the relationship obtained when the Michaelis-Menten term in (5) is replaced by a constant times CO_2 (linear dependence).

Discussion and Conclusions

Figures 19a and 19b and Table 3 summarize the results from the S450 and S750 atmospheric CO_2 scenarios of Figure 1 and the oceanic and terrestrial uptake scenarios of Figures 6 and 11. The combination of the atmospheric increase and uptake by the ocean and terrestrial biosphere gives an estimate of the allowable anthropogenic emissions in these scenarios. Note that in every scenario a large reduction of emissions is required in order to stabilize atmospheric CO_2 content. Perhaps the most important results of the study are that the estimated uptake by the terrestrial biosphere and ocean are of comparable magnitude and that, in combination, these two sinks greatly exceed the amount of CO_2 that remains in the atmosphere (Figures 19a and 19b and Table 3). The uncertainty in these estimates, which is partially illustrated here by the sensitivity of the terrestrial uptake to temperature and is better illustrated by the IPCC model comparison study (*Enting et al.* [1994]; see also *Wigley* [1993]), has major consequences for policy decisions on future fossil carbon utilization.

An additional result with important consequences is that owing to the nonlinearity of ocean chemistry and the photosynthetic response to increasing CO_2 levels, the airborne fraction is very sensitive to the maximum level to which CO_2 is allowed to rise as well as the rate at which CO_2 approaches this level (Figure 20). In both the terrestrial

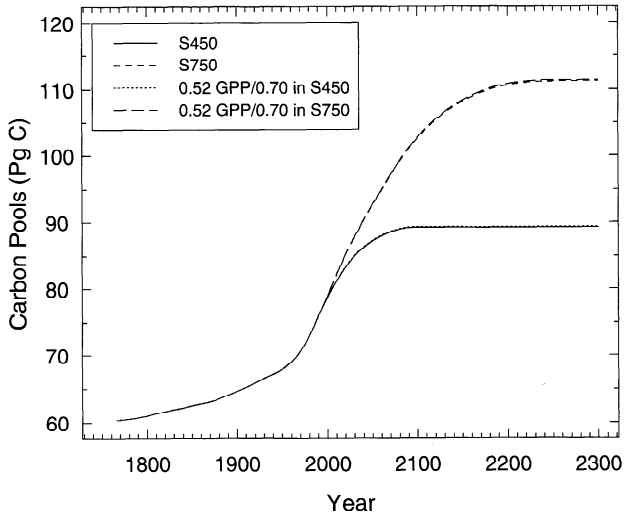

Figure 18. A plot showing that the time history of carbon in pool B (metabolic) can be represented by the simple function 0.52 GPP/0.70.

biosphere and ocean the fractional terrestrial and oceanic uptake capacity is significantly reduced as the CO_2 level increases and the rate of growth of CO_2 increases.

A great deal of research is needed in order to reduce the uncertainty of the carbon sinks. On the oceanic side, carbon chemistry is reasonably well understood and the use of ocean circulation tracers, such as radiocarbon, to calibrate our ocean models gives us confidence to about the 30% level in our model estimates of present oceanic uptake [e.g., *Siegenthaler and Sarmiento*, 1993], although *Hesshaimer et al.* [1994] have recently raised an important concern about the radiocarbon budget that suggests the oceanic uptake may be at the lower limit of the estimates. An important area where continued work is required is on observations to confirm the oceanic uptake by direct measurements. Also, the major uncertainty in future predictions is the possibility of large changes in ocean circulation occurring in response to global warming [e.g., *Manabe and Stouffer*, 1993]. In order to simulate the carbon cycle response to such changes, we require coupled atmosphere-ocean general circulation models, as well as models of ocean biology.

On the terrestrial biology side the nature of the terrestrial sink is almost entirely speculative at the present time. Its existence is inferred by differencing all the other terms in the carbon budget. The residual thus calculated, with its very large uncertainty, is among the most important constraints we have on the nature of the terrestrial uptake. The existence of such a sink is lent credence by the fact that its inferred magnitude can be reasonably well approximated by models with parameters that fall within the range of field and laboratory measurements (Table 2), as well as by tree ring observations, although the interpretation of the latter is controversial [*Auclair and Bedford*, 1993; Oechel, W. C., J. I. Holten, T. Callaghan, H. Elling, T. Gilmanov, B. Maxwell, U. Molau, O. Rogne, and B. Sveinbjornsson, *Global Change and Arctic Terrestrial Ecosystems. Proceedings of the Arctic Global Change Conference, Oppdal, Norway, August 21-26, 1993, Springer-Verlag, New York,* in press 1995; *D'Arrigo and Jacoby*, 1993]. The existence of a large terrestrial sink is also supported by measurements of carbon isotopes and atmospheric oxygen [e.g., *Quay et al.*, 1992; *Keeling and Shertz*, 1992].

The large future terrestrial uptake predicted by our models should be viewed primarily as an indication of the need for additional global change research on the terrestrial biosphere, rather than as a firm forecast. It is important to remember that the model is very simple. It does not discriminate among the different biomes, but rather attempts to capture the average

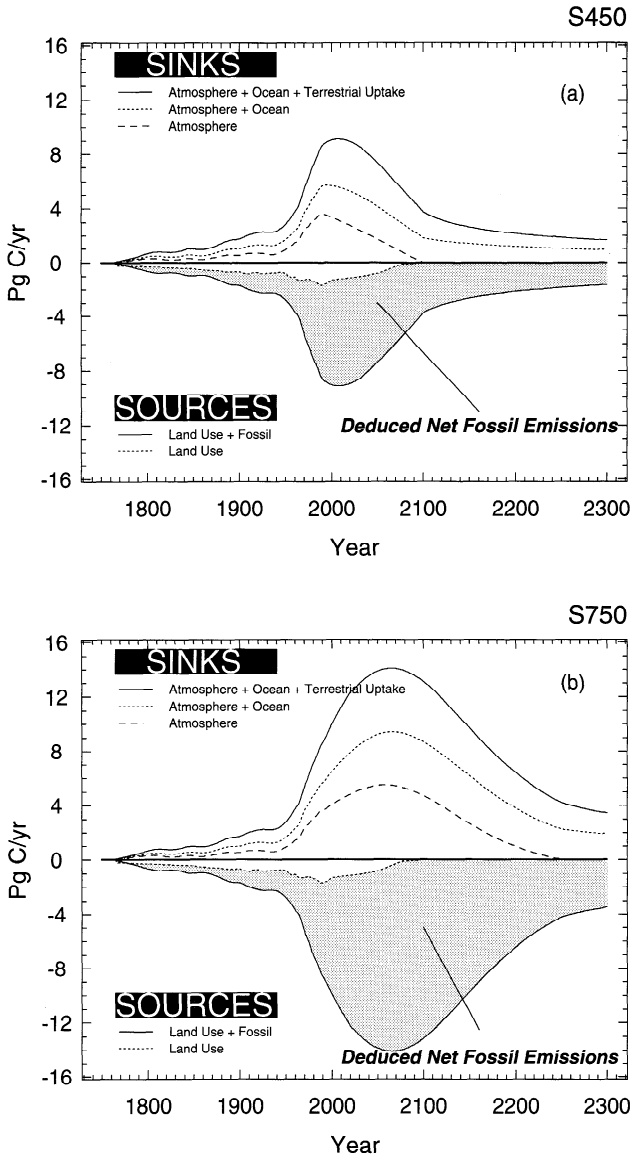

Figure 19. The cumulative uptake by the atmosphere, ocean, and terrestrial biosphere at the top of each diagram gives the total allowable sources shown in the bottom part. The land use flux estimate in the bottom of each diagram comes from *Enting et al.* [1994]. The difference between the estimated land use release and the total allowable emissions gives the deduced emissions that would be permitted from fossil fuel burning and cement use for (a) the S450 scenario and (b) the S750 scenario. In both cases the terrestrial uptake estimate does not include a correction for warming (see Figure 11 for an estimate of the impact of this).

Table 3. Results of S450 and S750 Simulations.

	Annual Increase, Pg yr^{-1}					Total, Pg
	Mean, Years 1980-1989	Year 2000	Year 2100	Year 2200	Year 2300	Years 1990-2300
			S450 Scenario			
Atmosphere	3.38	3.34	0.00	0.00	0.00	205
Ocean	1.83	2.32	1.80	1.16	0.90	497
Terrestrial Biosphere	2.23-2.65	2.54-3.38	1.14-1.95	0.40-0.98	0.26-0.73	322-554
Total	7.4-7.9	8.2-9.0	2.9-3.8	1.6-2.1	1.2-1.6	1024-1256
			S750 Scenario			
Atmosphere	3.38	4.05	4.70	0.95	0.00	842
Ocean	1.83	2.42	3.98	2.83	1.92	956
Terrestrial Biosphere	2.23-2.65	2.61-3.51	2.40-4.41	0.86-2.61	0.23-1.53	507-1029
Total	7.4-7.9	9.1-10.0	11.1-13.1	4.6-6.4	2.2-3.5	2305-2827

The range in terrestrial biosphere increases is for the models with the three following different temperature forcings: constant at the initial value, equilibrium warming due to the CO_2 increase, and equilibrium warming due to twice the CO_2 increase. The mean total increase of 7.4-7.9 Pg yr^{-1} in 1980-1989 agrees within the uncertainty with the estimated carbon release of 7.0±1.2 Pg yr^{-1} from fossil fuel burning and land use changes [*Sarmiento and Sundquist* [1992]. The agreement is even better when the actual temperature record prior to 1989 is used to force the terrestrial biosphere model.

response of the terrestrial biosphere as a whole. Regional responses obviously will deviate from the average. For example, the disproportionate warming of high latitudes predicted by most climate models [*Houghton et al.*, 1990] could result in disproportionate release of CO_2 from the large pools of undecomposed organic matter in these regions. Similarly, the model includes neither effects of nitrogen deposition nor changes in rainfall. Nitrogen deposition has received considerable attention in other studies [*Rasmussen et al.*, 1993; *Schindler and Bayley*, 1993], and we recognize the possibility that CO_2 may be serving as a proxy for nitrogen fertilization in fits of our model to the estimated time series of terrestrial uptake (or as a proxy for joint forcing by CO_2 and nitrogen), since fossil fuel consumption is a source for both. Future uptake of CO_2 by the terrestrial biosphere could also be curtailed if insufficient nitrogen is available to support increased production. Finally, changes in rainfall and evapotranspiration could obviously alter future patterns of terrestrial production [e.g., *Dai and Fung*, 1993].

Even so, there is considerable support for the mechanisms included in our model. Rates of photosynthesis, respiration and decay clearly do respond to temperature [*Raich et al.*, 1991; *Larcher*, 1980, *Raich and Schlesinger*, 1992]. Our estimates of these responses account for most of the interannual variability in the missing carbon from 1958 to the present and agree well with independent estimates from small-scale field and laboratory studies. Numerous experimental studies have shown an increase in carbon storage under elevated atmospheric CO_2 [*Bazzaz*, 1990; *Dahlman*, 1993; *Idso and Kimball*, 1993], and some dendrochronological studies have shown an increase in tree growth that mirrors the historic increase in atmospheric CO_2 [*Auclair and Bedford*, 1993; Oechel, W. C., J. I. Holten, T. Callaghan, H. Elling, T. Gilmanov, B. Maxwell, U. Molau, O. Rogne, and B. Sveinbjornsson, *Global Change and Arctic Terrestrial Ecosystems. Proceedings of the Arctic Global Change Conference, Oppdal, Norway, August 21-26, 1993, Springer-Verlag, New York,* in press 1995]. Our estimates of CO_2 responses both account for the long-term increase in the missing carbon and agree well with independent estimates from the experimental studies.

A major source of uncertainty in the terrestrial biosphere carbon sink is the likelihood of changes in the species composition of forests that may enhance the response of the terrestrial vegetation to the CO_2 increase and greenhouse warming by a very substantial amount (e.g., B. Bolker et al.,

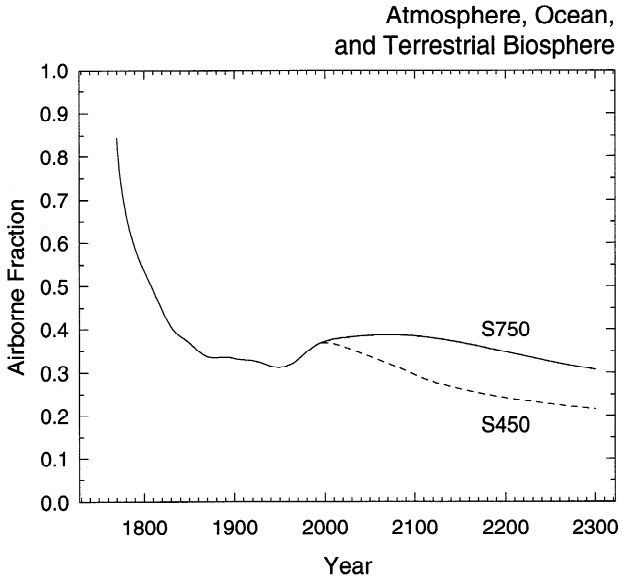

Figure 20. The airborne fraction for combined atmosphere, ocean, and terrestrial biosphere.

manuscript in preparation, 1994). Moreover, the terrestrial model employed in this study does not include limitation of uptake by factors other than light, atmospheric CO_2, and temperature. In particular, nitrogen limitation may severely constrain future terrestrial uptake if nitrogen deposition does not keep pace with nitrogen demand [cf. *Rasmussen et al.*, 1993 and *Schindler and Bayley*, 1993]. Additional studies of limitation of terrestrial production by mineral nutrients and water in the face of increased CO_2 and nitrogen deposition are essential to refine the forecasts presented here. However, large-scale experimental additions of CO_2 to terrestrial ecosystems (including forests) along gradients of water availability and anthropogenic nitrogen deposition would provide the most direct means to assess future terrestrial uptake of carbon.

Acknowledgments. We thank Peter Rayner and Simon Levin for their help in working through the dynamics of the oceanic and terrestrial biosphere responses. J. Olszewski assisted in the preparation of figures. This research was supported by the U. S. Department of Energy contract DEFG 02-90ER61052 (J.L.S. and C.L.Q.), the Seaver Foundation (S.W.P.), and the NOAA Geophysical Fluid Dynamics Laboratory through the courtesy of J. Mahlman and K. Bryan.

References

Alexander, R. C., and R. L. Mobley, Monthly average sea surface temperatures and ice pack limits on a 1° global grid, *Mon. Weather Rev.*, *104*, 143-148, 1976.

Amthor, J. S., The role of maintenance respiration in plant growth, *Plant, Cell Environ.*, *7*, 561-569, 1984.

Auclair, A. N. D., and J. A. Bedford, Forest depletion and accrual dataset, area and volume estimates, Revised Version 2, 15 Sept. 1993, Documentation File Report to OEPER/ORD, U.S. Environ. Prot. Agency, Washington, D. C., Science & Policy Assoc., Inc., W400, 1333 H St. NW, Washington, D. C., 1993.

Bacastow, R. B., J. A. Adams, C. D. Keeling, D. J. Moss, T. P. Whorf, and C. S. Wong, Atmospheric carbon dioxide, the Southern Oscillation, and the weak 1975 El Niño, *Science*, *210*, 66-68, 1980.

Bazzaz, F. A., The response of ecosystems to the rising global CO_2 levels, *Annual Rev. Ecol. Syst.*, *21*, 167-196, 1990.

Boden, T. A., R. J. Sepanski, and F. W. Stoss (Eds.), Trends '91: A compendium of data on global change, *Rep. ORNL/CDIAC-46*, vol. 700, Carbon Dioxide Inf. Anal. Cent., Oak Ridge Nat. Lab., Oak Ridge, Tenn., 1991.

Bolin, B., How much CO_2 will remain in the atmosphere?, in *The Greenhouse Effect, Climate Change and Ecosystems*, edited by B. Bolin, B. R. Doos, J. Jager, and R. A. Warrick, pp. 93-155, John Wiley & Sons, New York, 1986.

Broecker, W. S., T. H. Peng, G. Ostlund, and M. Stuiver, The distribution of bomb radiocarbon in the ocean, *J. Geophys. Res.*, *90*, 6953-6970, 1985.

Cannell, M. G. R., *World Forest Biomass and Primary Production Data*, Academic, San Diego, Calif., 1982.

Dahlman, R. C., CO_2 and plants: revisited, *Vegetatio*, *104/105*, 339-355, 1993.

Dai, A., and I. Y. Fung, Can climate variability contribute to the "missing" CO_2 sink?, *Global Biogeochem. Cycles, 7*, 599-609, 1993.

D'Arrigo, R. D., and G. C. Jacoby, Tree growth-climate relationships at the northern boreal forest tree line of North America: Evaluation of potential response to increasing carbon dioxide, *Global Biogeochem. Cycles*, *7*, 525-535, 1993.

Emmanuel, W. R., G. G. Killough, and J. S. Olson, Modeling the circulation of carbon in the worlds terrestrial ecosystem, in *Carbon Cycle Modelling, Scope 16*, edited by B. Bolin, pp. 335-353, John Wiley, New York, 1981.

Emmanuel, W. R., G. C. Killough, W. M. Post, and H. H. Shugart, Modeling terrestrial ecosystems in the global carbon cycle with shift in carbon storage capacity by land-use change, *Ecology*, *65*, 970-983, 1984.

Enting, I. G., T. M. L. Wigley, and M. Heimann, Assessment of the IPCC CO_2 Modelling Study, rep. *Tech. Pap. 31*, Div. of Atmos. Res., Commonwealth Sci. and Ind. Res. Organ., Melbourne, Victoria, Australia, 1994.

Esbensen, S. K., and Y. Kushnir, The heat budget of the global ocean: An atlas based on estimates from surface marine observations, *Clim. Res. Inst. Rep. 29*, Oreg. State Univ., Corvallis, 1981.

Friedli, H., H. Lötscher, H. Oeschger, U. Siegenthaler, and B. Stauffer, Ice core record of the $^{13}C/^{12}C$ ratio of atmospheric carbon dioxide in the past two centuries, *Nature*, *324*, 237-238, 1986.

Hansen, J., and S. Lebedeff, Global trends of measured surface air temperature, *J. Geophys. Res.*, *92*, 13,345-13,372, 1987.

Hellerman, S., and M. Rosenstein, Normal monthly wind stress over the world ocean with error estimates, *J. Phys. Oceanogr.*, *13*, 1093-1104, 1983.

Hesshaimer, V., M. Heimann, and I. Levin, Radiocarbon evidence for a smaller oceanic carbon dioxide sink than previously believed. *Nature, 370,* 201-203, 1994.

Houghton, J. T., G. J. Jenkins, and J. J. Ephraums, *Climate Change, The IPCC Scientific Assessment*, Cambridge University Press, New York, 1990.

Houghton, R. A., Changes in terrestrial carbon over the last 135 years, in *The Global Carbon Cycle, NATO ASI Ser.* vol. 115, edited by M. Heimann, pp. 139-157, Springer-Verlag, New York, 1993.

Idso, S. B., and B. A. Kimball, Tree growth in carbon dioxide enriched air and its implications for global carbon cycling and maximum levels of atmospheric CO_2, *Global Biogeochem. Cycles*, *7*, 537-555, 1993.

Keeling, C. D., and T. P. Whorf, Mauna Loa, in *Trends '91: A compendium of data on global change*, edited by T. A. Boden, R. J. Sepanski, and F. W. Stoss, *Rep. ORNL/CDIAC-46*, vol.. 700, pp. 12-14, Carbon Dioxide Info. Anal. Cent., Oak Ridge Nat. Lab., Oak Ridge, Tenn., 1991.

Keeling, C. D., R. B. Bacastow, A. F. Carter, S. C. Piper, T. P. Whorf, M. Heimann, W. G. Mook, and H. Roeloffzen, A three-dimensional model of atmospheric CO_2 transport based on observed winds, 1, Analysis of observational data, in *Aspects of Climate Variability in the Pacific and the Western Americas, Geophys. Monogr. Ser.* vol. 55, edited by D. H. Peterson, pp. 165-236, AGU, Washington D.C., 1989.

Keeling, R. F., and S. R. Shertz, Seasonal and interannual variations in atmospheric oxygen and implications for the global carbon cycle, *Nature*, *358*, 723-727, 1992.

Larcher, W., *Physiological Plant Ecology*. 2nd ed., Springer-Verlag, New York, 1980.

Levitus, S., Climatological atlas of the world ocean, *Prof. Pap. 13*, Nat. Oceanic and Atmos. Admin., Rockville, Md., 1982.

Maier-Reimer, E., and K. Hasselmann, Transport and storage of CO_2 in the ocean - An inorganic ocean circulation cycle model, *Clim. Dyn.*, *2*, 63-90, 1987.

Manabe, S., and R. J. Stouffer, Century-scale effects of increased atmospheric CO_2 on the ocean-atmosphere system, *Nature*, *364*, 215-218, 1993.

Marland, G., T. A. Boden, R. C. Griffin, S. F. Huang, P. Kanciruk, and T. R. Nelson, Estimates of CO_2 emissions from fossil fuel burning and cement manufacturing, based on the U.S. Bureau of Mines cement manufacturing data, *Rep. ORNL/CDIAC-25, NDP-030*, Carbon Dioxide Inf. Anal. Cent., Oak Ridge Nat. Lab., Oak Ridge, Tenn., 1989.

McGuire, A. D., J. M. Melillo, L. A. Joyce, D. W. Kicklighter, A. L. Grace, B. Moore III, and C. J. Vorosmarty, Interactions between carbon and nitrogen dynamics in estimating net primary productivity

for potential vegetation in North America, *Global Biogeochem. Cycles*, *6*, 101-124, 1992.

Metropolis, N., A. W. Rosenbluth, M. N. Rosenbluth, A. H. Teller, and E. Teller, Equation of state calculations for fast computing machines, *J. Chem. Phys.*, *21*, 1087-1092, 1953.

Neftel, A., H. Oeschger, J. Schwander, B. Stauffer, and R. Zumbrunn, Ice core measurements give atmospheric pCO_2 content during the past 40,000 years, *Nature*, *295*, 220-223, 1982.

Olson, J. S., V. A. Watts, and L. J. Allison, Carbon in live vegetation of major world ecosystems, *Rep. ORNL-5862*, Oak Ridge Nat. Lab., Oak Ridge, Tenn., 1983.

Parton, W. J., D. S. Schimel, C. V. Cole, and D. S. Ojma, Analysis of factors controlling soil organic levels of grasslands in the Great Plains, *Soil Sci. Soc. Am. J.*, *51*, 1173-1179, 1987.

Parton, W. J., J. W. B. Stewart, and C. V. Cole, Dynamics of C, N, P and S in grassland soils: A model, *Biogeochemistry*, *5*, 109-131, 1988.

Post, W. M., T. H. Peng, W. R. Emanuels, A. W. King, V. H. Date, and D. L. DeAngelis, The global carbon cycle, *Am. J. Sci.*, *78*, 310-326, 1990.

Quay, P. D., B. Tilbrook, and C. S. Wong, Oceanic uptake of fossil fuel CO_2: Carbon-13 evidence, *Science*, *256*, 74-79, 1992.

Raich, J. W., and W. H. Schlesinger, The global carbon dioxide flux in soil respiration and its relationship to vegetation and climate, *Tellus*, *Ser. B*, *44B*, 81-99, 1992.

Raich, J. W., E. B. Rastetter, J. M. Melillo, D. W. Kicklighter, P. A. Steudler, B. J. Peterson, A. L. Grace, B. Moore, and C. J. Vorosmaity, Potential net primary productivity in South America: Application of a global model., *Ecol. Appl.*, *1*, 399-429, 1991.

Rasmussen, L., T. Brydges, and P. Mathy (Eds.), *Experimental Manipulation of Biota and Biogeochemical Cycling in Ecosystems*, Committee of European Communities, Brussels, 1993.

Rastetter, E. B., M. G. Ryan, G. R. Shaver, J. M. Melillo, K. J. Nodelhoffer, J. E. Hobbie, and J. D. Aber, A general model describing response of the C and N cycles in terrestrial ecosystem to changes in CO_2, climate and N deposition, *Tree Physiol.*, *9*, 101-126, 1991.

Ryan, M. G., Effects of climate changes on plant respiration, *Ecol. Appl.*, *1*, 157-167, 1991.

Sarmiento, J. L., J. C. Orr, and U. Siegenthaler, A Perturbation simulation of CO_2 uptake in an ocean general circulation model, *J. Geophys. Res.*, *97*, 3621-3646, 1992.

Sarmiento, J. L., and E. T. Sundquist, Revised budget for the oceanic uptake of anthropogenic carbon dioxide, *Nature*, *356*, 589-593, 1992.

Schimel, D. S., T. G. Kittel, and W. J. Parton, Terrestrial biogeochemical cycles: Global interactions with the atmosphere and hydrology, *Tellus*, *Ser. A*, *43A*, 188-203, 1991.

Schindler, D. W., and S. E. Bayley, The biosphere as an increasing sink for atmospheric carbon: Estimates from increased nitrogen deposition, *Global Biogeochem. Cycles*, *7*, 717-733, 1993.

Siegenthaler, U., and J. L. Sarmiento, Atmospheric carbon dioxide and the ocean, *Nature*, *365*, 119-125, 1993.

Siegenthaler, U., H. Friedli, H. Loetscher, E. Moor, A. Neftel, H. Oeschger, and B. Stauffer, Stable-isotope ratios and concentration of CO_2 in air from polar ice cores, *Ann. Glaciol.*, *10*, 1-6, 1988.

Szymura, J. M., and N. H. Barton, Genetic analysis of a hybrid zone between the fire-bellied toads near Cracow in southern Poland, *Evolution*, *40*, 1141-1159, 1986.

Taylor, J. A., and J. Lloyd, Sources and sinks of atmospheric CO_2, *Aust. Journal of Botany*, *40*, 407-418, 1992.

Toggweiler, J. R., and B. Samuels, Is the magnitude of the deep outflow from the Atlantic Ocean actually governed by southern hemisphere winds?, in *The Global Carbon Cycle*, edited by M. Heimann, pp. 333-366, Springer-Verlag, New York, 1993.

Toggweiler, J. R., K. Dixon, and K. Bryan, Simulation of radiocarbon in a coarse-resolution world ocean model., 1, Steady state prebomb distributions, *J. Geophys. Res.*, *94*, 8217-8242, 1989.

Wanninkhof, R., Relationship between wind speed and gas exchange over the ocean, *J. Geophys. Res.*, *97*, 7373-7383, 1992.

Wigley, T. M. L., Balancing the carbon budget. Implications for projections of future carbon dioxide concentration changes, *Tellus*, Ser. B, *45B*, 209-235, 1993.

Zinke, P. U., A. G. Stangenberger, A. G. Post, W. M. Emmanuel, and J. S. Olson, Worldwide organic soil carbon and nitrogen data, *Rep. 2212*, Environ. Sci. Div., Oak Ridge Nat. Lab., Oak Ridge, Tenn., 1986.

C. Le Quéré and J.L. Sarmiento, Atmospheric and Oceanic Sciences Program, Princeton University, P.O. Box CN710, Sayre Hall, Princeton, NJ 08544.

S.W. Pacala, Department of Ecology and Evolutionary Biology, 101 Eno Hall, Princeton, NJ 08542.

(Received March 1, 1994; revised June 30, 1994;
accepted July 7, 1994)